Effect of wing-box structure on the optimum wing outer shape

A. Elham
a.elham@tudelft.nl
Delft University of Technology
Delft, The Netherlands

M. J. L. van Tooren
University of South Carolina
Columbia, USA

ABSTRACT

A new method for wing shape optimisation is presented, in which the wing shape is optimised not only for the best aerodynamic properties but also for minimum structural weight. An advanced structural sizing method for wing structural weight estimation is developed. The method is based on elementary, physics based analyses of simplified structure to determine the amount of required material to resist the applied loads. The sizing loads are determined based on the airworthiness regulations using advanced aerodynamic analysis tools. In this new weight estimation method, the effect of wing outer (aerodynamic) shape on the wing-box structural weight is taken into account. A mathematical equation is derived, which relates the wing-box structural weight to the wing outer shape. The weight estimation method is validated for several existing passenger aircraft. A series of optimisations is performed to optimise the wing shape for a general objective function, which includes both aerodynamic and structural properties of the wing. The aircraft fuel weight is used as the objective function. Different structures are tested both metal and composite ones. The latter includes different composite layups. In order to find the effect of the internal structure on the optimum wing outer shape, the design lift coefficient is assumed to be constant for all the test cases. The results of the optimisations showed that the optimum wing shape is depending on the structural concept (metal alloys versus different composite layups) for different internal structures.

Paper No. 3953. Manuscript received 24 January 2013, revised version received 17 June 2013, accepted 12 August 2013.

https://doi.org/10.1017/S0001924000008903 Published online by Cambridge University Press

1.0 INTRODUCTION

Constrained multivariable optimisation techniques are widely used for the design and optimisation of aerofoil sections as well as three-dimensional wings. These methods try to find the optimum aerodynamic shape by the combined use of numerical optimisation techniques and computational fluid dynamics solvers. Aerodynamic optimisation aims to reduce the drag of an aircraft for a given lift, thereby increasing the aircraft aerodynamic efficiency and therefore reducing the required fuel weight for a specific mission[4,13,19,22]. Beside aerodynamic efficiency, the aircraft fuel efficiency is also affected by the aircraft weight. Therefore the potential for improvements in aircraft fuel consumption can not be fully realised using pure aerodynamic shape optimisation without considering the effect of the aircraft shape on its weight. Hence a multidisciplinary design optimisation (MDO) approach is needed. This requires a weight estimation method sensitive to aerodynamic shape changes.

Aircraft wing structural weight can be estimated using various methods with different level of fidelity i.e. different classes: from simple statistics based equations up to detailed finite element analysis (FEA) of the structure. In general the lower the fidelity, the more the method is based on statistics. Examples of such low fidelity wing weight estimation methods are presented by Torenbeek[21], Raymer[16] and Howe[7]. Although these methods enable designers to assess the effect on weight caused by certain design choices, e.g., due to a given wing planform layout, their level of sensitivity is not enough to be used in a wing shape optimisation. For instance these methods capture the effect of the wing outer shape on the weight only via the value of the maximum profile thickness. In addition to that, the effect of the structural design solution, such as the number and position of spars and ribs in the wing, effect of the material properties, as well as the effect of the aerodynamic load distribution on the structural weight cannot be evaluated.

High class methods, which use FEA to size various components of the primary structure, are sensitive to more design variables. Examples of this kind of methods are presented by Droegkamp[6], Bindolino[3], Laban[12], Hurlimann[9] and Sensmeier[17]. Although these methods are more accurate than the statistical methods and provide better design sensitivity, the time required to prepare a FE model and perform the analysis can be quite large, certainly, orders of magnitude larger than computing the simple empirical equation. Besides that, these methods require very large amount of detailed data about the geometry and material, which is usually not available in the early design stage. This limits their use in MDO in the early steps of preliminary design.

In the 1950s a new set of weight estimation methods was introduced[5,18] based on elementary strength/stiffness analysis of the wing-box structure, augmented by experimental and statistical data. These methods, which are called quasi-analytical methods, have the low computational cost of low class methods, but can achieve levels of accuracy comparable to the FEA based methods. After more than half a century these kind of methods are still widely used. Examples of these methods for wing weight estimation are presented by Torenbeek[20], Macci[14], Ardema[2] and Kelm[11].

To enable wing shape optimisation for minimum fuel weight, a quasi-analytical wing weight estimation method is developed, which has two main key advantages: high level of accuracy and sensitivity to wing outer shape (aerofoil). This method is used together with an aerodynamic solver for multidisciplinary wing shape optimisation, to capture the effect of wing outer shape on both wing drag and wing structural weight. Beside that, using the sensitivity of the weight estimation method to the material properties, the effect of material (e.g. aluminum alloys or CFRP) choice on the optimum aerodynamic shape of a wing becomes clear. Doing so, the wing outer shape can be optimised not only for the aerodynamic aspects, but also for the structural weight, which will result in a more realistic optimum design for minimum fuel consumption.

https://doi.org/10.1017/S0001924000008903 Published online by Cambridge University Press

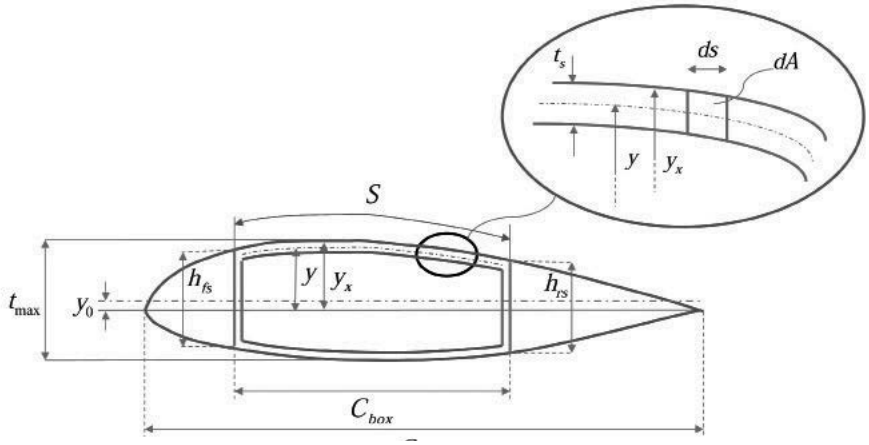


Figure 1. Wingbox structure.

The proposed method is integrated with an aerodynamic solver to optimise the wing outer shape for various objective functions. The results of a pure aerodynamic optimisation (drag minimisation) and a pure structural optimisation (weight minimisation) are compared to the results of a full MDO for fuel minimisation. Beside that, the effect of using various materials used to construct the wing-box on the optimum wing outer shape is investigated.

2.0 PROPOSED METHODS EMPLOYED FOR PRELIMINARY STRUCTURAL SIZING OF WING TORSION-BOX

This section describes the methods employed for initial sizing of the wing torsion-box structure in order to have an accurate structural weight estimation. For the preliminary sizing, the torsion-box structure can be simplified using equivalent panels. In this way the upper skin, stringers and spar caps are modeled with an equivalent upper panel. In a similar way the lower skin, stringers and spar caps are modeled with an equivalent lower panel. Spar webs are modeled separately with vertical panels (Fig. 1). The upper and lower panels are sized to withstand bending moments while the spars webs are sized based on shear loads.

2.1 Sizing method for the upper and lower panels

In a wing-box with homogeneous material in each equivalent panel, the axial stress in each element ($dA = t_s ds$) of the upper and the lower panels is determined as a function of the applied bending moment (M), section second moment of area (I) and the distance between that element and the bending moment axis of the section ($y - y_0$):

$$\sigma = \frac{M(y - y_0)}{I} \quad \ldots (1)$$

https://doi.org/10.1017/S0001924000008903 Published online by Cambridge University Press

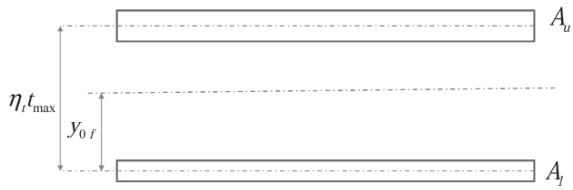


Figure 2. Equivalent flat panels located at effective distance.

The location of the bending moment axis (y_0 in Fig. 1) is defined as:

$$y_0 = \frac{\oint y t \mathrm{d}s}{\oint t \mathrm{d}s} \quad \ldots (2)$$

Using Fig. 1 y in Equation (1) for the upper and lower panels is defined as:

$$\begin{aligned} y_u &= y_{x_u} - t_{s_u}/2 \\ y_l &= y_{x_l} + t_{s_l}/2 \end{aligned} \quad \ldots (3)$$

If the panel thickness is assumed to be constant along the wing-box chord, the axial stress is maximum at the element with maximum y_x. Therefore the stress distribution in the panels can be presented as a function of the aerofoil geometry:

$$\begin{aligned} \sigma_u &= \frac{(y_u - y_0)}{y_{max_u}} \sigma_{max_u} \\ \sigma_l &= \frac{(y_l - y_0)}{y_{max_l}} \sigma_{max_l} \end{aligned} \quad \ldots (4)$$

where y_{max} is the maximum of $y - y_0$. In order to simplify the sizing method, the upper and lower panels are replaced with two flat panels located at an effective distance (Fig. 2). Replacing the curved panels with the flat ones allows to size the panels assuming uniform stress distribution. The effective distance ($\eta_t t_{max}$) is a fraction of the aerofoil maximum thickness (t_{max}). Parameter η_t should be calculated such that the total bending moment in the curved and flat panels is equal (see Section 2.4).

Using Equation (2) the location of the bending moment axis of the flat panels shown in Fig. 2 is calculated:

$$y_{0_f} = \frac{A_u}{A_u + A_l} \eta_t t_{max} \quad \ldots (5)$$

Where A_u and A_l are the area of the equivalent upper and lower panels respectively. Using Equation (5) the proper values of $y - y_0$ in Equation (1) for the upper and lower panels are calculated:

$$\begin{aligned} y_{u_f} - y_{0_f} &= \eta_t t_{max} \frac{A_l}{A_u + A_l} \\ y_{l_f} - y_{0_f} &= \eta_t t_{max} \frac{A_u}{A_u + A_l} \end{aligned} \quad \ldots (6)$$

https://doi.org/10.1017/S0001924000008903 Published online by Cambridge University Press

The second moment of area (I) of the section shown in Fig. 2 is derived as follows:

$$I = A_u(\eta_t t_{max}\frac{A_l}{A_u + A_l})^2 + A_l(\eta_t t_{max}\frac{A_u}{A_u + A_l})^2 = \eta_t^2 t_{max}^2\left(\frac{A_u A_l}{A_u + A_l}\right) \quad \ldots (7)$$

Substituting Equations (6) and (7) in Equation (1), the minimum required areas of the upper and lower panels are determined:

$$A_u = \frac{M/\sigma_{max_u}}{\eta_t t_{max}} \quad \ldots (8)$$

$$A_l = \frac{M/\sigma_{max_l}}{\eta_t t_{max}} \quad \ldots (9)$$

where σ_{maxu} and σ_{maxl} are the maximum allowable stresses in the upper and lower panels respectively (see Section 2.3). The thicknesses of the curved panels are determined using $t_s = A/S$, where S is the length of the curved panels:

$$t_{s_u} = \frac{M/\sigma_{max_u}}{\eta_t t_{max} S_u} \quad \ldots (10)$$

$$t_{s_l} = \frac{M/\sigma_{max_l}}{\eta_t t_{max} S_l} \quad \ldots (11)$$

2.2 Sizing method for spars webs

The areas of the spars webs are calculated using the shear stress analysis. The shear flow in the spar web is the sum of the shear flow due to the torsional moment and the shear flow due to the vertical loads.

The shear flows due to the vertical load in the front and rear spars are estimated implementing the method presented by Howe[8]:

$$q_{v_{fs}} = \frac{h_{fs}}{(h_{fs}^2 + h_{rs}^2)}V \quad \ldots (12)$$

$$q_{v_{rs}} = \frac{h_{rs}}{(h_{fs}^2 + h_{rs}^2)}V \quad \ldots (13)$$

where h_{fs} and h_{rs} are the heights of the front and rear spars respectively and V is the total vertical force.

The shear flow due to the torsional moment is calculated as follows:

$$q_t = \frac{T}{2A_{box}} \quad \ldots (14)$$

where T is the torsional moment and A_{box} is the enclosed area of the wing box. The torsional moment should be calculated about the elastic axis (shear center for a 2D section). The location of the shear center is calculated using the method presented by Megson[28]. In this method the location of the shear center is determined using the condition that a shear load acting through the

https://doi.org/10.1017/S0001924000008903 Published online by Cambridge University Press

shear center of a section produces zero twist:

$$\frac{\mathrm{d}\theta}{\mathrm{d}z} = \frac{1}{2A_{box}} \oint \frac{q}{Gt} \mathrm{d}s = 0 \Rightarrow \oint \frac{q}{Gt} \mathrm{d}s = 0 \quad \ldots (15)$$

Using Equation (15) the chordwise location of the shear center is found by applying a vertical shear force, V, through the y axis:

$$x_{sc} = -\frac{1}{V} \oint \frac{q}{Gt} \mathrm{d}s \quad \ldots (16)$$

From Equations (15) and (16) one can find that the location of the shear center is a function of the panels thickness (t). So it should be determined in an iterative process.

Finally, the thickness of each spar web is calculated using the total shear flow ($q = q_v + q_t$) and the maximum allowable shear stress (τ_{max}):

$$t_w = \frac{q}{\tau_{max}} \quad \ldots (17)$$

2.3 Determination of the allowables

2.3.1 Metal alloys

The lower panel is assumed to be under tension in positive load factors. In the early design phase of the aircraft, when this method is supposed to be used, the knowledge about the design is not sufficient to account for fatigue and associated crack propagation phenomena. Therefore, ignoring the effect of fatigue and considering the use of monolithic and homogeneous metal panels, the allowable stress in the lower panel is assumed equal to the material tensile yield stress F_{t_y}.

For the upper panel, which is under compression in positive load factors, the maximum allowable stress is selected as the minimum of the compressive yield stress (F_{c_y}) and the buckling stress. The buckling stress of a stiffened panel under compression can be calculated using the stiffened panel efficiency method[15]:

$$\sigma_{max_b} = F\left(\frac{PE}{L}\right)^{1/2} \quad \ldots (18)$$

where F is the stiffened panel efficiency factor, P is the load intensity, E is the Young's modulus and L is the rib pitch. The load intensity in the upper panel is equal to:

$$P = \frac{\sigma A_u}{C_{box}} \quad \ldots (19)$$

Substituting Equation (8) in (19), the load intensity is represented in such a way that $P = \frac{M}{\eta_t t_{max} C_{box}}$.

Using this value for P, the maximum allowable stress is determined as follows:

$$\sigma_{max_u} = min\left(F_{c_y}, F\sqrt{\frac{ME}{\eta_t t_{max} C_{box} L}}\right) \quad \ldots (20)$$

https://doi.org/10.1017/S0001924000008903 Published online by Cambridge University Press

Eventually the maximum allowable shear stress can be estimated using the method presented in Ref. 23:

$$\tau_{max} = \frac{F_{t_y}(L) + F_{t_y}(LT) + F_{c_y}(L) + F_{c_y}(LT)}{4} \times \frac{2F_{s_u}}{F_{t_u}(L) + F_{t_u}(LT)} \quad \ldots (21)$$

where subscripts t, c and s denote tension, compression and shear respectively, y and u denote yield and ultimate stresses respectively, and L and LT denote the longitudinal and long transverse direction of the material respectively.

The shear buckling stress in a plate (such as a spar web) is determined as follow:

$$\tau_{max_b} = K_s E \left(\frac{t_w}{h_s} \right)^2 \quad \ldots (22)$$

The factor K_s can be determined from the available charts such as the one presented in Ref. 15. The spars web are designed for post buckling. In this approach the webs must not buckle under the loads up to e.g. 40% of the maximum applied load. For higher load, they are allowed to buckle. From Equation (22) one can find that the shear buckling stress of a spar web is a function of the web thickness (t_w) and the spar height (h_s). The spar height is known from the aerofoil geometry, while the web thickness should be determined as a function of the allowable shear stress (see Equation 17). So some iteration is required to determine the webs thicknesses.

2.3.2 Composite materials

The strength of a composite structure takes a range of values as a result of material variability, environmental effects, and sensitivity to damage. In preliminary design, the so-called cut-off strain can be used to size composite structures[8,10]. The cutoff strains are determined based on the worst of all situations[10]. The allowables for composite materials are calculated using these cutoff strains in combination with the so-called 10% rule[24]. The 10% rule allows to estimate the mechanical properties of a laminate from the ply properties and the percentages of plies in each direction. Implementing this approach, the maximum allowable stress in the lower panel is calculated using Equation (23):

$$\sigma_{maxl} = E_x \varepsilon_t \quad \ldots (23)$$

where E_x is the laminate stiffness in x direction and ε_t is the cut-off tensile strain.

For the upper panel, the maximum allowable compressive stress is calculated using the same type of equation as (23), where a cut-off compressive strain (ε_c) is used instead of ε_t. The buckling stress is calculated using the method presented by Tetlow[36]:

$$\sigma_{maxb} = 0 \cdot 725 F (E_{x0}{}^2 Z)^{1/4} \sqrt{\frac{P}{L}} \quad \ldots (24)$$

where Z is calculated using the following equations:

$$Z = \frac{E_x K}{E_{x0}} \quad \ldots (25)$$

https://doi.org/10.1017/S0001924000008903 Published online by Cambridge University Press

Table 1
Suggested values for cut-off strains

Tensile	Compressive	Shear
0·005	0·0045	0·006

$$K = \frac{\pi^2}{6(1-\nu_{xy}\nu_{yx})E_{x0}}\left((E_xE_y)^{1/2} + \nu_{xy}\frac{E_y}{2} + \nu_{yx}\frac{E_x}{2} + 2(1-\nu_{xy}\nu_{yx})G_{xy}\right)$$

Concerning the spars webs, the maximum allowable shear stress is calculated as follows:

$$\tau_{max} = G_{xy}\varepsilon_s \quad \ldots (26)$$

where G_{xy} is the laminate shear stiffness and ε_s is the cutoff shear strain.

The required laminate properties in Equations (23), (25) and (26) are calculated using the 10% rule[24] as follows:

$$\begin{aligned} E_x &= (0\cdot1 + 0\cdot9\frac{m}{100})E_{x0} \\ E_y &= (0\cdot1 + 0\cdot9\frac{100-m-n}{100})E_{x0} \\ G_{xy} &= (0\cdot028 + 0\cdot234\frac{n}{100})E_{x0} \\ \nu_{xy} &= \nu_{yx} = \frac{1}{1+4(\frac{100-m-n}{n})} \end{aligned} \quad \ldots (27)$$

where m is the percentage of plies at 0 degree, n is the percentage of plies at ±45° and E_{x0} is the stiffness of the unidirectional lamina along the principal direction.

The cut-off strains can be determined using angle minus longitudinal (AML) plots method[29]. The AML is the percentage of plies in ±45° minus the percentage of plies in 0°($n - m$). In order to create an AML plot, laminates of different layups, which provide a range of AML, are drilled or impacted and tested to failure in various situations: under room temperature, hot/wet, and cold/dry conditions. The allowable strains are derived from test data are plotted as a function of AML. These plots can be used to determine the cut-off strains as a function of the composite layup. Example of AML plot is presented in Ref. 29. If such plots are not available, the cut-off strains provided in Table 1 can be used.

2.4 Method for calculation of the effective distance

The wing box effective distance is an important parameter, which relates the structural weight of the wing to the wing outer shape. Shanley[18] proposes the following method to calculate η_t as a function of the aerofoil geometry:

$$\eta_t = \frac{1}{Nt_{max}(z_{max} - \frac{t_s}{2})}\sum_{n=1}^{N}[z_{u_n}^2 + z_{l_n}^2 - t_s(z_{u_n} - zl_n) + \frac{t_s}{2}] \quad \ldots (28)$$

https://doi.org/10.1017/S0001924000008903 Published online by Cambridge University Press

where z is the aerofoil ordinate measured from the bending moment axis $(y_x - y_0)$ in Fig. 1 and N is the number of elements used to discretise the wing-box panels. It should be noted that, in the equation above, the upper and the lower panels are assumed to have the same thickness t_s.

Torenbeek[20] suggested a simplified empirical equation to estimate the value of η_t as a function of the aerofoil maximum thickness and the heights of the front (h_{fs}) and rear spar (h_{rs}):

$$\eta_t \approx \frac{1}{3}\left(1 + (h_{fs}/t_{max})^2 + (h_{rs}/t_{max})^2\right) - 0{\cdot}025 \qquad \ldots (29)$$

In this equation, it is assumed that the thickness of the upper and lower panels are the same and equal to 2·5% of the maximum thickness of the aerofoil. Torenbeek also proposed that η_t can be assumed equal to 0·8 when the knowledge of designers is not enough to use Equation (29).

Elham *et al*[26] performed some case studies to investigate the effect of different values of η_t for wing weight estimation of transport aircraft. According to that work increasing η_t from 0·8 to 1 causes about 12% error in wing weight estimation of the Boeing 747 type aircraft. This large influence of η_t on wing weight estimation requires a precise attention for the estimation of η_t. A method developed by the authors[40] is used to calculate the effective distance.

This method is based on the rationale that the total bending moment in the curved equivalent panels (Fig. 1) should be equal to the total bending moment in the flat equivalent plates (Fig. 2). The total bending moment in the box with curved panels is equal to:

$$M_c = \oint \sigma y \mathrm{d}A = \sum_{n=1}^{N} \sigma_{u_n} (y_{u_n} - y_0) t_{s_u} \mathrm{d}s_{u_n} + \sum_{n=1}^{N} \sigma_{l_n} (y_{l_n} - y_0) t_{s_l} \mathrm{d}s_{l_n} \qquad \ldots (30)$$

Substituting Equation (4) in (30), the total bending moment in the curved panels is calculated:

$$M_c = \frac{\sigma_{max_u}}{y_{max_u}} \sum_{n=1}^{N} (y_{u_n} - y_0)^2 t_{s_u} \mathrm{d}s_{u_n} + \frac{\sigma_{max_l}}{y_{max_l}} \sum_{n=1}^{N} (y_{l_n} - y_0)^2 t_{s_l} \mathrm{d}s_{l_n} \qquad \ldots (31)$$

The bending moment in the flat plates is presented as following:

$$M_f = \sigma_{u_{max}} A_u (\eta_t t_{max} - y_{0_f}) + \sigma_{l_{max}} A_l \, y_{0_f} \qquad \ldots (32)$$

Assuming that t_{s_u} and t_{s_l} are constant along the chord, A_u and A_t can be replaced with $A_u = t_{s_u} S_u$ and $A_t = t_{s_l} S_l$. Substituting Equation (5) in Equation (32), the equation of the total bending moment in the flat plates is reduced to:

$$M_f = \eta_t t_{max} \left(\frac{t_{su} Su \, t_{sl} S_l}{t_{su} S_u + t_{sl} S_l} \right) (\sigma_{maxu} + \sigma_{maxl}) \qquad \ldots (33)$$

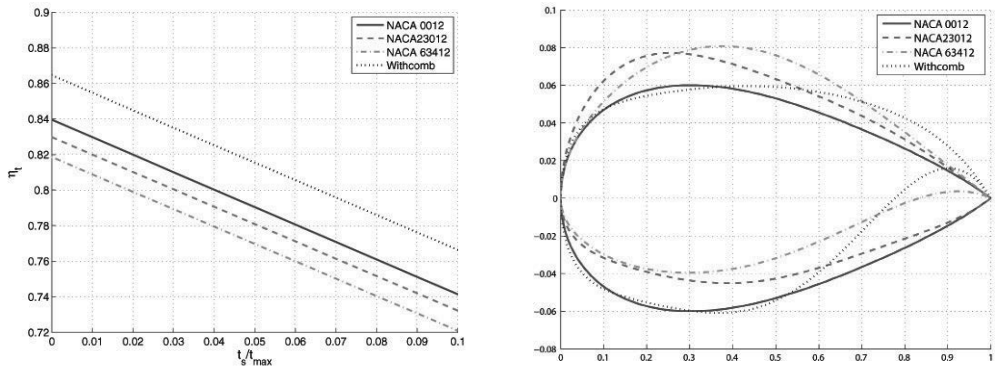
Using $M_c = M_f$, after some reductions, η_t is calculated:

$$\eta_t = \frac{1}{t_{max}} \left(\frac{1}{S_u \, y_{max_u}} \sum_{n=1}^{N} (y_{u_n} - y_0)^2 \mathrm{d}s_{u_n} + \frac{1}{S_l \, y_{max_l}} \sum_{n=1}^{N} (y_{l_n} - y_0)^2 \mathrm{d}s_{l_n} \right) \qquad \ldots (34)$$

The effect of the aerofoil shape on the value of η_t is shown in Fig. 3. Four different aerofoils with the same maximum thickness to chord ratio equal to 0·12 are tested.

From Fig. 2 one can observe that the value of η_t for the Withcomb aerofoil is about 5·5% higher

https://doi.org/10.1017/S0001924000008903 Published online by Cambridge University Press



(a) η_t as function of panel thickness

(b) Aerofoils geometry

Figure 3. η_t for various aerofoils with the maximum thickness to chord ratio equal to 0·12.

Table 2
Validation results of wing weight estimation method.

Aircraft	Maximum take-off weight (kg)	Error of wing weight estimation (%)	optimum wing box weight / wing total weight
Fokker 50	20,820	–1·75	0·34
Fokker 100	43,090	4·26	0·40
Boeing 737-200	52,390	1·23	0·41
Boeing 727-300	95,028	–1·85	0·53
Airbus A300-600R	170,500	1·67	0·54
Airbus A330-300	217,000	0·8	0·65
Boeing 777-200	242,670	3·61	0·59

than η_t for the NACA 63412 aerofoil. Considering Equations (8) and (9), such difference in the value of η_t can cause more than 5% difference in the weight of wing-box skins, stringers and spars caps. This example demonstrates the importance to derive a η_t value that is specific to the actual geometry of the wing, whereas assuming a fixed η_t value (such as 1 or 0·8) would make the weight estimation both inaccurate and not design sensitive.

3.0 VALIDATION

The total wing weight is calculated by adding the non-optimum and the secondary weights to the calculated optimum wing-box weight. The non-optimum weights are the weight penalties due to joints, attachments, cutouts etc. The secondary weights are the weights of the secondary structures such as fixed leading and trailing edges, flaps, slats ailerons and spoilers.

The optimum wing-box weight is calculated using the presented method. The sizing loads are computed using the aerodynamic loads and the relief loads. The aerodynamic loads are calculated

https://doi.org/10.1017/S0001924000008903 Published online by Cambridge University Press

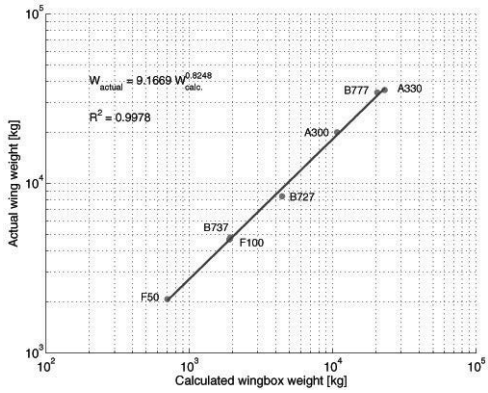


Figure 4. Correlation between the calculated wing-box weight and the actual wing weight.

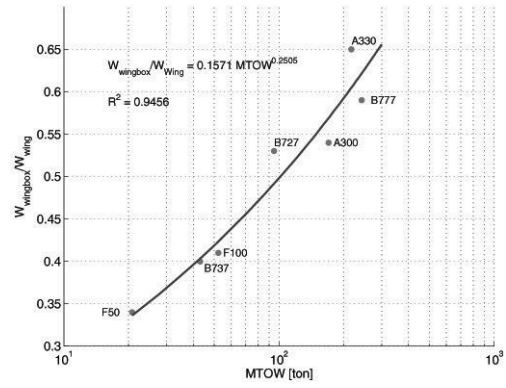


Figure 5. Regression between the ratio of the optimum wing-box weight to the wing total weight and the aircraft MTOW.

using a vortex lattice method (VLM). Both manoeuver and gust loads are calculated for a quasi-equilibrium condition (the dynamic response of the aircraft is ignored), and the critical one is used. The relief loads due to the wing weight, fuel weight and the weight of the wing mounted engines are taken into account. The ribs weight, the non-optimum weights (weight penalties due to joint, attachments, cutouts, etc.) and the secondary weights (weights of fixed leading edge and trailing edge, flaps, slats, ailerons and spoilers) are calculated using the empirical equations presented by Torenbeek[20].

The weight prediction method has been validated using the actual weight of various aircraft from different manufacturers, size and category. The required data of those aircraft (geometrical and structural data and the actual weight breakdown) were gathered from literature[15,32,30,35] and also from private communication with industries. The results are presented in Table 2. The error of wing weight estimation is calculated as follows:

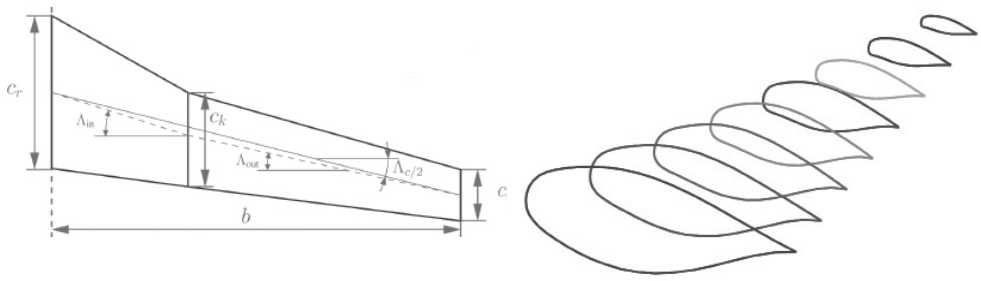
$$error = \frac{W_{calc} - W_{actual}}{W_{calc}} \qquad \ldots (35)$$

The validation results show an average error of 2·10% and a standard deviation of 1·99%. These values are comparable to the best existing FEA based weight estimation methods. The accuracy is also independent from the aircraft type, size and manufacturer. The computational time required for each weight estimation is in the order of 30 seconds, and includes the time to generate the wing geometrical model, compute the aerodynamic loads, and perform the required iterations.

A simple regression analysis (see Fig. 4) has been performed to derive a relationship between the wing box weight contribution computed analytically (i.e., the weight of the upper and lower skin panels, stringers, spar caps and webs) and the actual total wing weight. The result of the power regression is given in Equation (36):

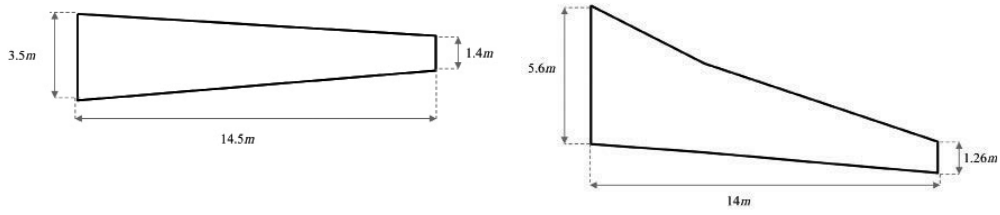
$$W_{total} = 9 \cdot 1669\, W_{wingbox}^{0 \cdot 8248} \qquad \ldots (36)$$
$$R^2 = 0 \cdot 9978$$

https://doi.org/10.1017/S0001924000008903 Published online by Cambridge University Press



(a) Wing planform (b) Wing shape

Figure 6. Definition of the wing planform and shape.



(a) Subsonic turbofan aircraft (b) Transonic turbofan aircraft

Figure 7. Wing planform geometry.

Using this approach the aircraft wing weight can be estimated using only the analytical methods and no empirical equation is required. This reduces the amount of required input data. This approach is very suitable in early design stages, where some of the required input data (e.g. data about the high lift devices and control surfaces) are not available.

From Table 2 one can find that the ratio of the wing-box weight to the wing total weight increases by increasing the aircraft MTOW. Figure 5 shows the regression between the ratio of the optimum wing-box weight to the wing total weight and the aircraft MTOW.

4.0 WING SHAPE OPTIMISATION

As mentioned in Section 1, in order to achieve minimum fuel consumption, a multidisciplinary optimisation is required. The goad of the present research is to optimise the wing shape for minimum fuel consumption, without assuming that this is achieved when L/D is maximised. The wing shape is referred only to the wing outer aerodynamic shape (aerofoil) and not to the wing planform, which is considered fixed during the optimisation (see Fig. 6).

The wing shape affects both the wing aerodynamic efficiency (lift over drag ratio) and the wing structural weight. Therefore a pure aerodynamic shape optimisation will not result in a realistic optimum shape. In order to find the real optimum, the effect of wing shape on the wing structural weight must be taken into account as well. A series of optimisations has been executed to optimise the wing shape for various objective functions.

https://doi.org/10.1017/S0001924000008903 Published online by Cambridge University Press

Two test cases are considered for wing shape optimisation: a typical turboprop (subsonic) and a typical turbofan (transonic) passenger aircraft. Figure 7 shows the planform geometry of the wings of those aircraft. In all of the optimisations the planform geometry is frozen and the wing outer shape (aerofoil) is optimised.

The wing shape is parametrised using the class shape transformation (CST) method[27]. CST is symbolically described as follows:

$$\zeta(\psi) = C_{N2}^{N1}(\psi) \cdot S(\psi) \quad \ldots (37)$$

where $\xi = y/c$ and $\Psi = x/c$. C_{N2}^{N1} and $S(\Psi)$ present the class and shape functions respectively. The class function expresses the basis class of shapes:

$$C_{N2}^{N1}(\psi) = (\psi)^{N1}\,(1-\psi)^{N2} \quad \ldots (38)$$

For a round nose and pointed aft end aerofoil, $N1$ and $N2$ are equal to 0·5 and 1 respectively. The shape function is a Bernstein polynomial representation which describes the permutation around this basic shape:

$$S(\psi) = \sum_{i=0}^{p} \overline{P}_i B_{i,p}(\psi) \quad \ldots (39)$$

where p is the order of the Bernstein polynomial, $\overline{P}_i$ is the vector of control points and $B_{i,p}(\Psi)$ are the Bernstein polynomials of degree p.

Aerofoils at four different spanwise positions are parametrised using ten design variables for each (40 in total). Both the upper and lower aerofoil surfaces are parametrised using five control points. These sections are located at the root, one third and two third of the semi span and the tip.

The sequential quadratic programming (SQP) algorithm of the MATLAB optimisation toolbox[39] is used as the optimiser.

4.1 Aerodynamic solver

A CFD code called MATRICS-V[38] is selected as the aerodynamic solver. The MATRICS-V flow-solver is based on fully-conservative full-potential outer flow in quasi-simultaneous interaction with an integral boundary-layer method on the wing. The code can be used to treat fixed angle-of-attack as well as fixed lift analysis problems, and features:

- Three-dimensional laminar and turbulent boundary-layers.
- Two options for the laminar-to-turbulent boundary-layer transition.
- Capability to model considerable boundary-layer separation.
- Shock capturing for supersonic/subsonic shock waves consistent with Rankine-Hugoniot relations.
- Multigrid acceleration of flow solver.

The automatic special-purpose grid generator of MATRICS-V facilitates the use of high-resolution, single-block standard grids of C-O topology, both for low-mounted and high-mounted wings. The MATRICS-V flow solver has been validated using wind tunnel data and flight test data. As can be concluded from Figs 8 and 9, MATRICS-V provides results that are in good agreement with experimental and in-flight test data.

https://doi.org/10.1017/S0001924000008903 Published online by Cambridge University Press

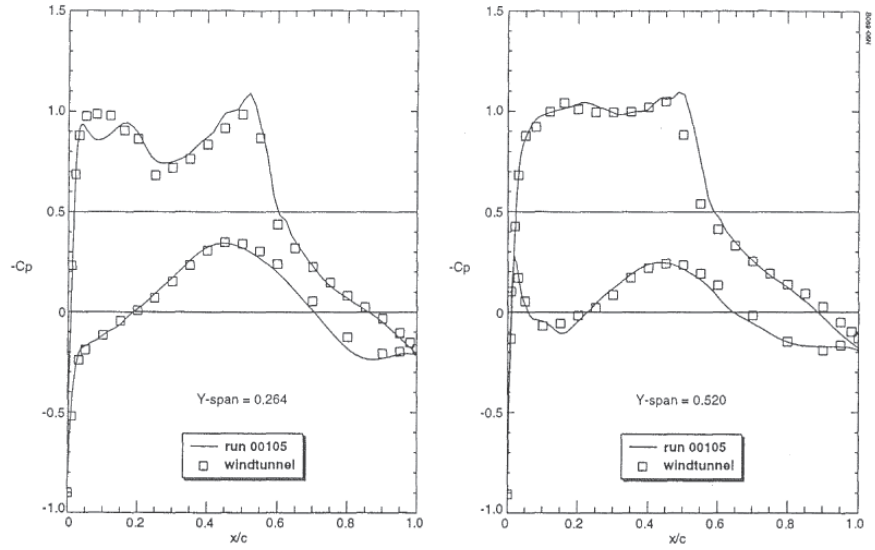


Figure 8. Comparison of MATRICS-V and wind tunnel measured chordwise pressure distribution on two wing section of Fokker 100 wing/body configuration at $M_\infty = 0{\cdot}779$, $\alpha = 1{\cdot}03°$, $Re = 3 \times 10^6$. Source: NLR[40].

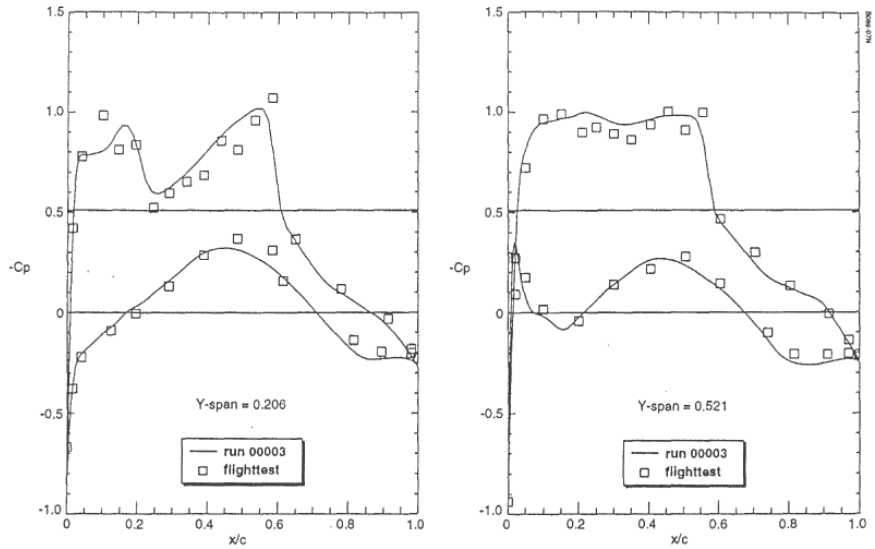
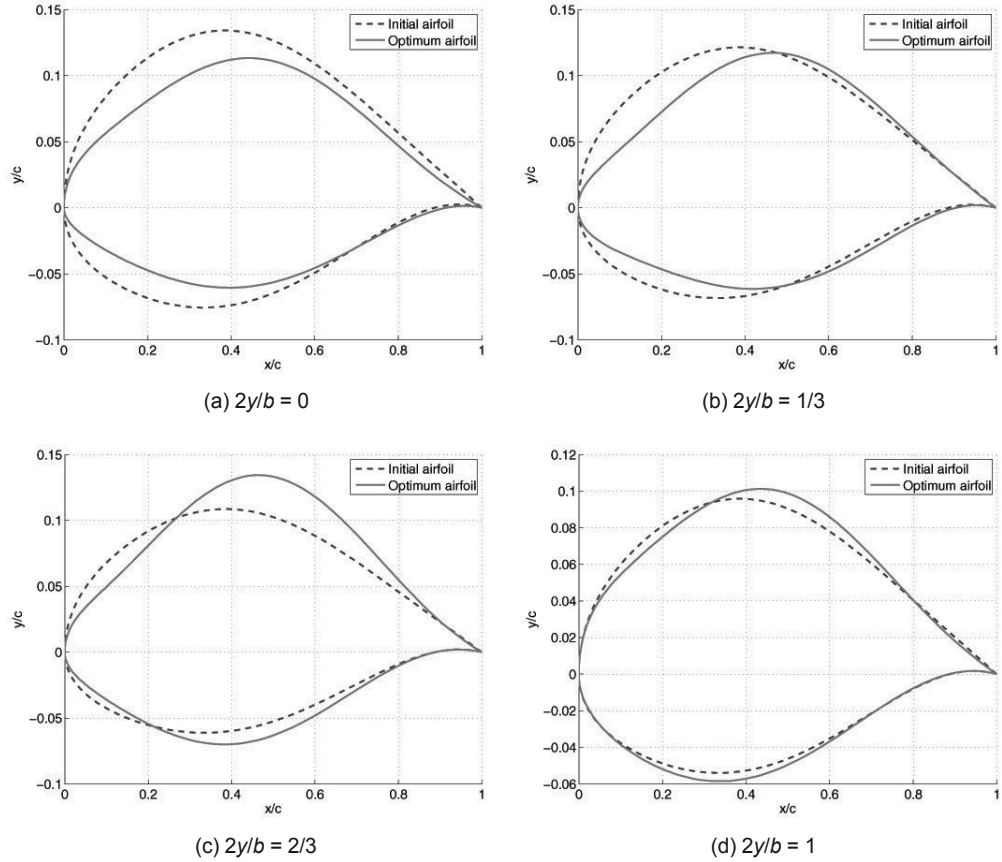


Figure 9. Comparison of MATRICS-V and in flight measured chordwise pressure distribution on two wing section of Fokker 100 wing/body configuration at $M_\infty = 0{\cdot}775$, $\alpha = 1{\cdot}0°$, $Re = 35 \times 10^6$. Source: NLR[40].

https://doi.org/10.1017/S0001924000008903 Published online by Cambridge University Press

Table 3
Aerodynamic parameters of subsonic and transonic wings.

	Subsonic wing	Transonic wing
C_L	0·35	0·45
Mach number	0·55	0·77
Reynolds number	$1{\cdot}6 \times 10^7$	$2{\cdot}5 \times 10^7$



(a) 2y/b = 0 (b) 2y/b = 1/3

(c) 2y/b = 2/3 (d) 2y/b = 1

Figure 10. Wing sections of the subsonic wing optimised for minimum drag.

4.2 Wing drag minimisation

In the first optimisation case, an aerodynamic drag minimisation task is considered. The optimisation is formulated as follows:

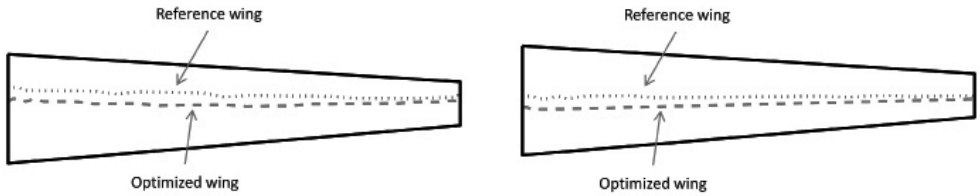
$$min \quad F(X)$$

$$\text{where} \quad F = C_{D_{wing}}$$

$$X = \text{wing geometry parameters}$$

$$s.t. \quad C_L = C_{L_{des}}$$

https://doi.org/10.1017/S0001924000008903 Published online by Cambridge University Press



(a) Wing upper surface (b) Wing lower surface

Figure 11. Boundary layer transition line of the reference and the optimised wings.

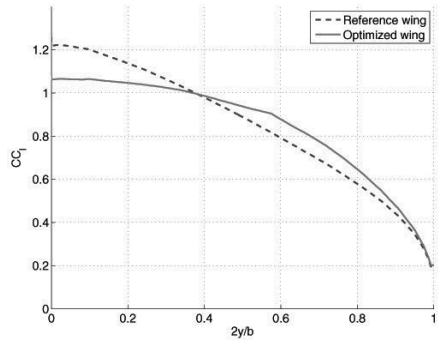


Figure 12. Wing lift distribution.

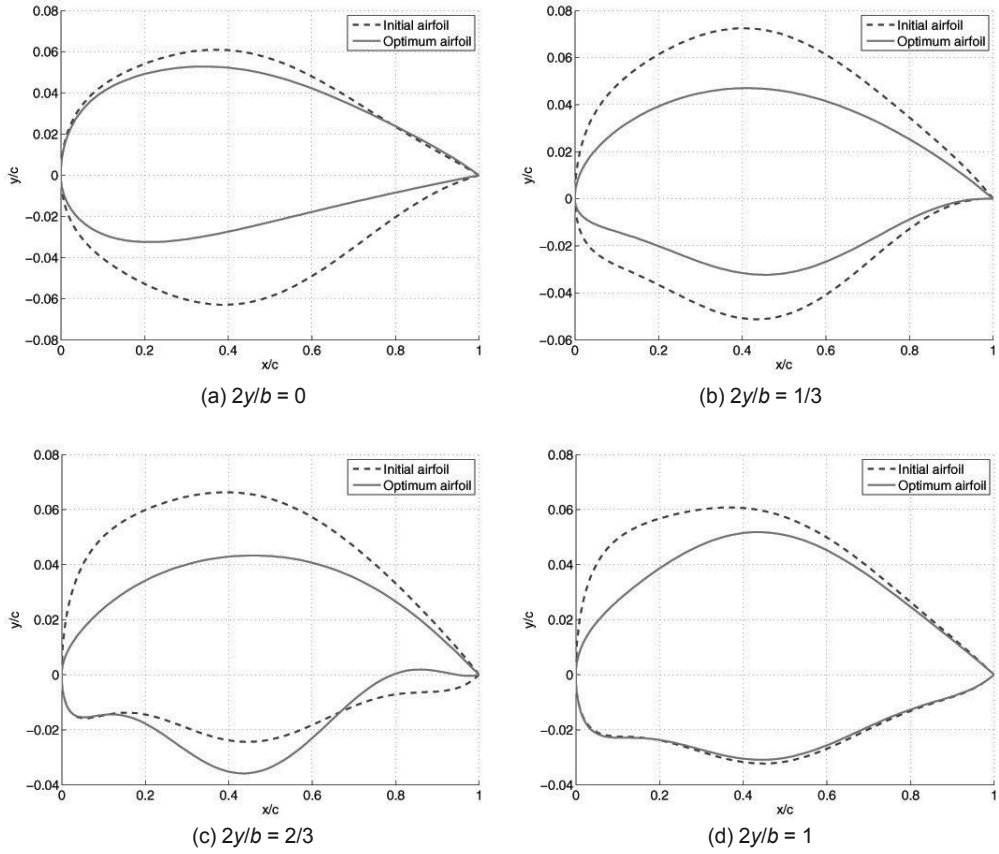
$$(t/c)_{max_{i_{lower}}} \leq (t/c)_{max_i} \leq (t/c)_{max_{i_{upper}}}$$

where $C_{D_{wing}}$ is the wing drag coefficient and $C_{L_{des}}$ is the design lift coefficient, which is considered equal to 0·35 and 0·45 for the subsonic and transonic aircraft respectively. The aerofoils thickness to chord ratio is limited between 0·10 and 0·25 for the subsonic aircraft and between 0·08 and 0·18 for the transonic aircraft. The aerodynamic parameters of the wings are summarised in Table 3.

The aerofoils of the subsonic wing optimised for minimum drag are shown in Fig. 10. The optimised wing has 16% lower drag than the reference (initial) wing, however the wight of wing skin, stringers and spars is 16% higher. 85% of the drag reduction is achieved by reducing the viscous drag and the remaining 15% is due to the reduction of the induced drag. The viscous drag reduction is acheived by shifting the transision line toward the trailing edge to have more laminar flow on the upper and lower sides of the wing (see Fig. 11).

The induced drag reduction is achieved as a result of a lift distribution closer to the elliptical lift distribution, which results in the minimum possible induced drag[1]. The wing lift distributions ($C\ C_l$) for the reference wing and the optimised wing are shown in Fig. 12. The changes in the lift distribution are achieved only by changing the aerofoils shape, because the wing planform parameters (such as span, taper ratio, sweep angle etc) and the wing twist distributions (which is mainly used for adjusting the lift distribution) are not defined as design variables. From Fig. 12 one can observe that the optimiser decreased the inboard lift by decreasing the thickness and camber of the root aerofoil (see Fig 9) and increased the outboard lift (near $2y/b \approx 0{\cdot}6$) by increasing the thickness and camber of the local aerofoil (see Fig. 9).

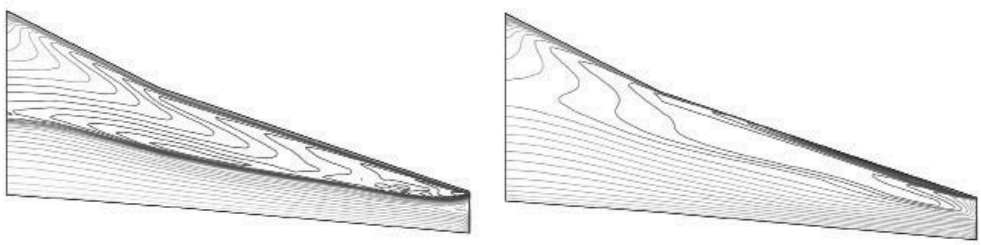
https://doi.org/10.1017/S0001924000008903 Published online by Cambridge University Press



(a) $2y/b = 0$ (b) $2y/b = 1/3$

(c) $2y/b = 2/3$ (d) $2y/b = 1$

Figure 13. Wing sections of the transonic wing optimised for minimum drag.



(a) Reference wing (b) Optimised wing

Figure 14. Contour of pressure coefficient on the wing upper surface.

The aerofoils of the transonic wing optimised for minimum drag are shown in Fig. 13. The thickness to chord ratio of all the optimised aerofoils is reduced to 8%, the minimum allowed value for the thickness to chord ratio. As a results, a 27% drag reduction is achieved. This drag reduction is achieved by 51% reduction in the wave drag, 47% reduction in the viscous drag and

https://doi.org/10.1017/S0001924000008903 Published online by Cambridge University Press

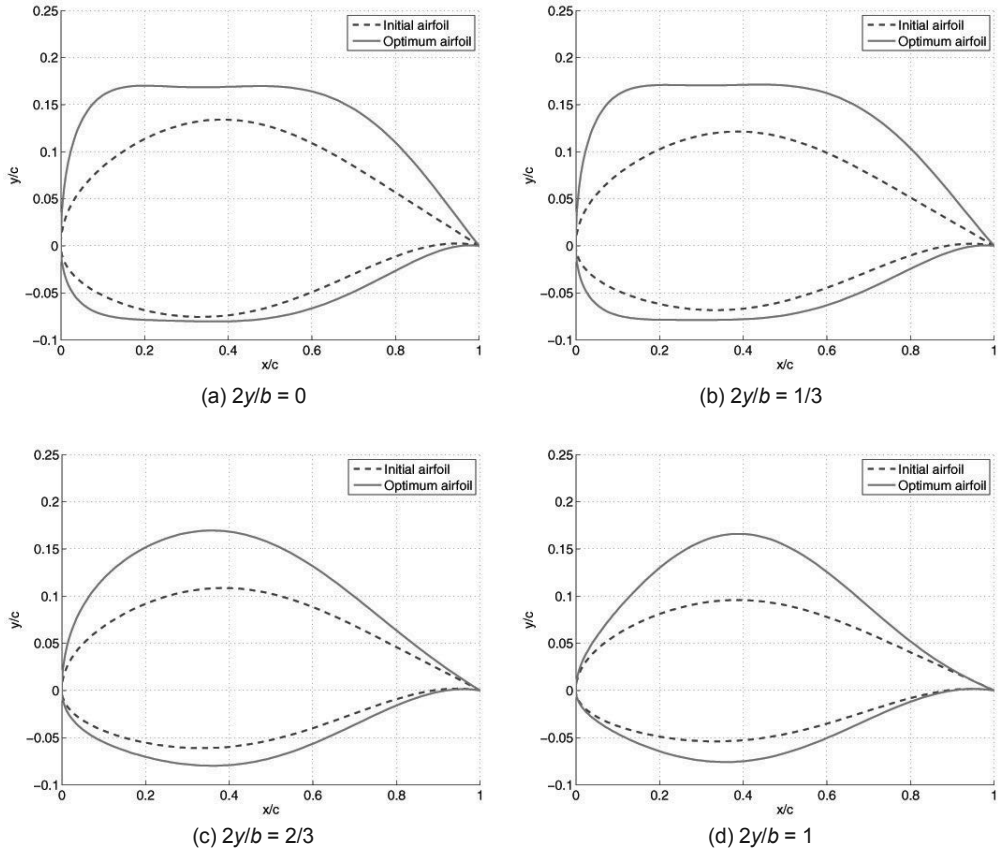


Figure 15. Wing sections of the subsonic wing optimised for minimum structural weight.

2% reduction in the induced drag. The contours of the pressure coefficient on the upper surfaces of the reference and the optimised wings are shown in Fig. 14. From this figure one can observe a strong shock wave along the wing span on the upper surface of the reference wing, while the optimised wing is shock free. Although by this optimisation a large amount of drag reduction is achieved, the wing-box structural weight is increased by 33%.

4.3 Wing structural weight minimisation

In the second optimisation task, the wing structural weight is considered as objective function. The secondary weights (weight of flaps, slats, etc.) are assumed to be constant, while the wing-box optimum weight is assumed to be altered with the wing outer shape. In order to estimate the primary weight, the front and rear spars are assumed to be located at 20% and 60% of the chord respectively. The rib pitch for both wings is assumed to be 60cm. The stiffened panel efficiency factor (see Section 2.3) is selected equal to 0·96 (according to *Z* type stringer). The material used in the lower equivalent panel is Aluminium alloy Al-2024-T3, while the material in the other panels (upper equivalent panel, front and rear spars webs) is Al-7075-T6. The method prescribed in Section 2 is used to estimate the wing structural weight. The aerodynamic loads are calculated using a vortex lattice code called AVL[25].

https://doi.org/10.1017/S0001924000008903 Published online by Cambridge University Press

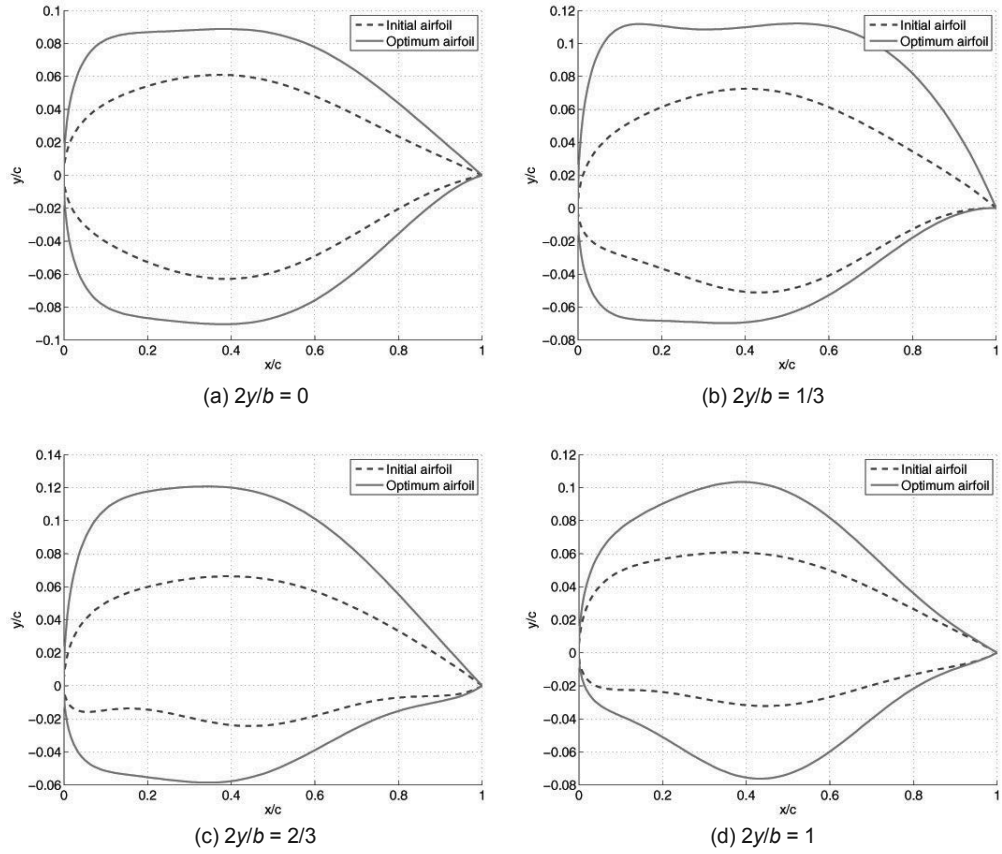


Figure 16. Wing sections of the transonic wing optimised for minimum structural weight.

Figures 15 and 16 show the optimised aerofoils for both subsonic and transonic wings. In both cases, the optimiser increased the aerofoils thicknesses up to the maximum allowed value for the thickness to chord ratio (25% for the subsonic and 18% for the transonic aircraft). In addition to that, the optimiser tried to maximise the value of $\eta_t t_{max}$ (see Equations 8 and 9 by increasing the aerofoil effective distance (see Figs 17 and 18). The effective distance of an aerofoil is maximum ($\eta_t = 1$) for a rectangular wing-box. From Figs 15 and 16 one can observe that the wing-box part of the aerofoils near the root have almost rectangular shape. Near the tip, the value of the bending moment and the shear force are low, hence the thickness of the equivalent panels are usually determined based on the minimum gauge thickness. In that case the thicknesses of the equivalent panels are independent of the aerofoil shape. As it is the case in Figs 15 and 16, where the wing-box of the aerofoils near the tip are not completely rectangular ($\eta_t < 1$).

In this optimisation, the wing-box structural weight is reduced by 22% and 38% for the subsonic and the transonic aircraft respectively.

The spanwise variation of $\eta_t t_{max}$ for three wings (the reference wing, the wing optimised for minimum drag and the wing optimised for minimum weight) is shown in Figs 17 and 18 for both subsonic and transonic aircraft.

https://doi.org/10.1017/S0001924000008903 Published online by Cambridge University Press

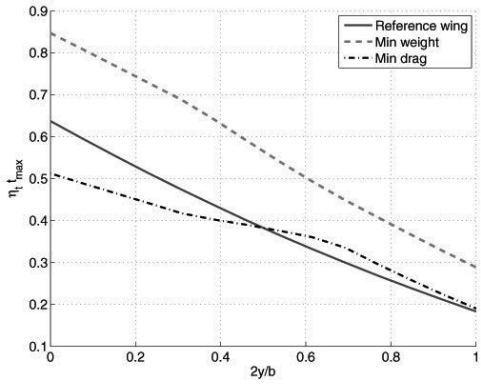


Figure 17. Spanwise variation of $\eta_t t_{max}$ for three different wings for subsonic aircraft.

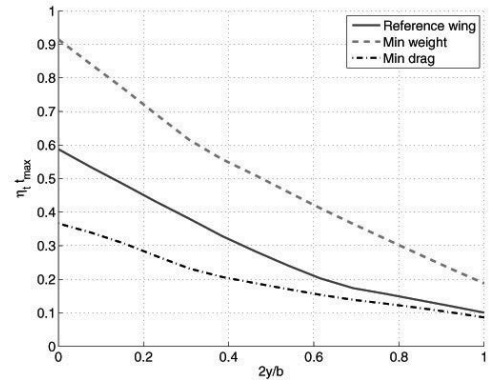


Figure 18. Spanwise variation of $\eta_t t_{max}$ for three different wings for transonic aircraft.

4.4 Fuel weight minimisation

The third optimisation case is in fact a full multidisciplinary design optimisation (MDO) task, in which both aerodynamic and structural properties of the wing are taken into account in the objective function and not as constraints on the variables. In this optimisation case, the aircraft fuel weight is minimised, while the wing weight is kept equal or less than the wing weight of the reference aircraft. The optimisation is defined as follows:

$$min \quad F(X)$$

$$\text{where} \quad F = W_{fuel}$$

$$X = \text{wing geometry parameters}$$

$$s.t. \quad C_L = C_{L_{des}}$$

$$W_{wing} \leq W_{wing_{ref}}$$

$$(t/c)_{max_{i_{lower}}} \leq (t/c)_{max_i} \leq (t/c)_{max_{upper}}$$

The values of the design lift coefficient and the lower and upper bounds for the aerofoil thickness to chord ratios are the same as the values used in Section 4.2.

A constraint is added to the optimisation to keep the wing weight equal or less than the initial wing weight. This constraint is added to avoid any increase in aircraft direct operating cost due to increasing the aircraft structural weight. Without such a constraint on the wing weight, the optimisation may result in a wing resulting lower fuel weight but with higher structural weight. Reducing the aircraft fuel weight will result in lower fuel cost, but increasing the aircraft structural weight will increase some other components of the aircraft direct operating cost (such as maintenance cost, depreciation cost etc.), which are functions of the aircraft structural weight.

The method presented by Roskam[31], is used to calculate the aircraft fuel weight. In this method the required fuel for the cruise is calculated using the Breguet range equation, while some statistical factors are used to estimate the fuel weight of the other segments of the flight mission, see Table 4. Each fuel weight fraction M_{ff_i} indicates the ratio of the total aircraft weight (all up weight) at the end of each flight segment to the total aircraft weight at the beginning of that segment.

The total fuel weight fraction indicated the consumed fuel as a ratio of the total aircraft weight

https://doi.org/10.1017/S0001924000008903 Published online by Cambridge University Press

Table 4
Fuel fractions for each segment in a typical flight mission, suggested values by Roskam[31]

Fuel weight fraction, M_{ff_i}	Turboprop aircraft	Turbofan aircraft
1. Start & warm-up	0·990	0·990
2. Taxi	0·995	0·990
3. Take-off	0·995	0·995
4. Climb	0·985	0·980
5. Cruise	*Calculated*	*Calculated*
6. Descent	0·985	0·990
7. Landing, taxi & shutdown	0·995	0·992

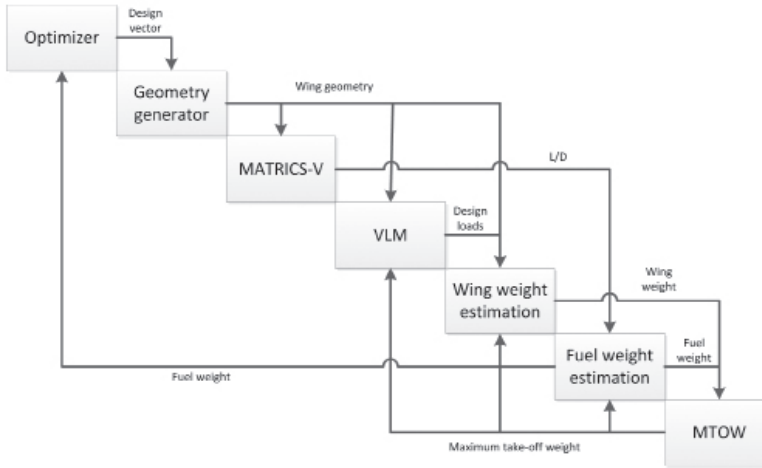


Figure 19. Design structure matrix of the MDO.

at the end of the flight mission to the total aircraft weight at the beginning.

$$M_{ff} = M_{ff_1} \cdot M_{ff_2} \cdot \ldots \cdot M_{ff_n} \quad \ldots (40)$$

Hence, the fuel weight can be determined including a 5% of the total fuel weight as reserve fuel using the following equation:

$$W_f = 1 \cdot 05\left(1 - M_{ff}\right)W_{to} \quad \ldots (41)$$

The effect of structural weight on the aircraft fuel weight can be observed from Equation (41). The aircraft take-off weight includes the aircraft structural weight. Increasing the aircraft structural weight increases the aircraft take-off weight, hence the weight of the required fuel for a given mission.

From Equation (41) one can find that the fuel weight is a function of the aircraft take-off weight, which is a function of the fuel weight and the structural weight (including the wing weight). Therefore some iteration is required to converge to a solution. The design structural matrix (DSM) of the MDO is shown in Fig. 19.

https://doi.org/10.1017/S0001924000008903 Published online by Cambridge University Press

Table 5
Weights of the optimised aircraft.

	Subsonic aircraft		Transonic aircraft	
	Reference aircraft	Optimised aircraft	Reference aircraft	Optimised aircraft
W_{fuel} [kg]	4,045	3,960	7,312	6,607
W_{wing} [kg]	2,067	2,054	4,677	4,677
MTOW [kg]	20,867	20,768	43,144	42,440

From Fig. 19 one can find that there are two aerodynamic solvers included in the MDO framework. One high fidelity solver, MATRICS-V, and a lower fidelity vortex lattice method (VLM). The MATRICS-V is used to calculate the wing drag, which is required for fuel weight estimation, while the VLM is used to estimate the aerodynamic loads needed for wing structural sizing and weight estimation.

The drag of the other aircraft components (e.g. fuselage, tail) is assumed to be constant. The payload weight and all components of the aircraft operational empty weight (OEM) except the wing structural weight are assumed to be constant. Although the aircraft MTOW is altering during the optimisation, the cruise lift coefficient is assumed to be constant and therefore there is no feedback from MTOW to the MATRICS-V block. The author's experience shows that the maximum reduction in aircraft MTOW in such an MDO is about 2% (if the optimisation starts with a well designed wing, which is the case in this MDO). This amount of change in MOTW does not change the wing design lift coefficient seriously (ΔC_L equal to 0·006 for subsonic and 0·0034 for transonic aircraft, where the design lift coefficient is defines as $C_{L_{des}} = \frac{\sqrt{\text{MTOW} \times \text{MZFW}}}{q\, S_w}$).

Therefore, in order to speed up the optimisation the wing lift coefficient is assumed to be constant and equal to those valued presented in Table 3. Besides, fixing the aircraft cruise lift coefficient is useful to investigate the effect of wing internal structure on the wing optimum outer shape, which is the goal of this research. Changing the aircraft structure changes the aircraft total weight and hence the required lift coefficient for cruise flight. It is not surprising to see two wings optimised for different lift coefficients have different shapes. In that case the difference in the shapes is mainly caused by the difference in their design lift coefficients. Fixing the lift coefficient can guarantee that the difference in the optimum aerofoils shapes is not caused by the lift coefficient but by the internal structure.

In order to calculate the required fuel for cruise the aircraft total drag is required. The wing drag is estimated using the MATRICS-V code, while the other drag components (such as fuselage drag, tail drag, interference drag etc.) are assumed to be the same as those for the initial aircraft. In fact the wing drag is the only component of the aircraft drag, which is assumed to be affected by the wing shape during the optimisation.

Table 5 presents the results of the MDO for minimising the aircraft fuel weight. The resulted optimum wing shape is compared to the optimum shapes for minimum drag and minimum weight in Figs 20 and 21.

From Table 5 it can be concluded that for the subsonic aircraft only 2% reduction in fuel weight is achieved, while for the transonic aircraft the reduction in the fuel weight is about 10%. The wing weight for the subsonic aircraft is slightly reduced however for the transonic case it is the same as the wing weight of the reference aircraft. The position of the transition line on the upper

https://doi.org/10.1017/S0001924000008903 Published online by Cambridge University Press

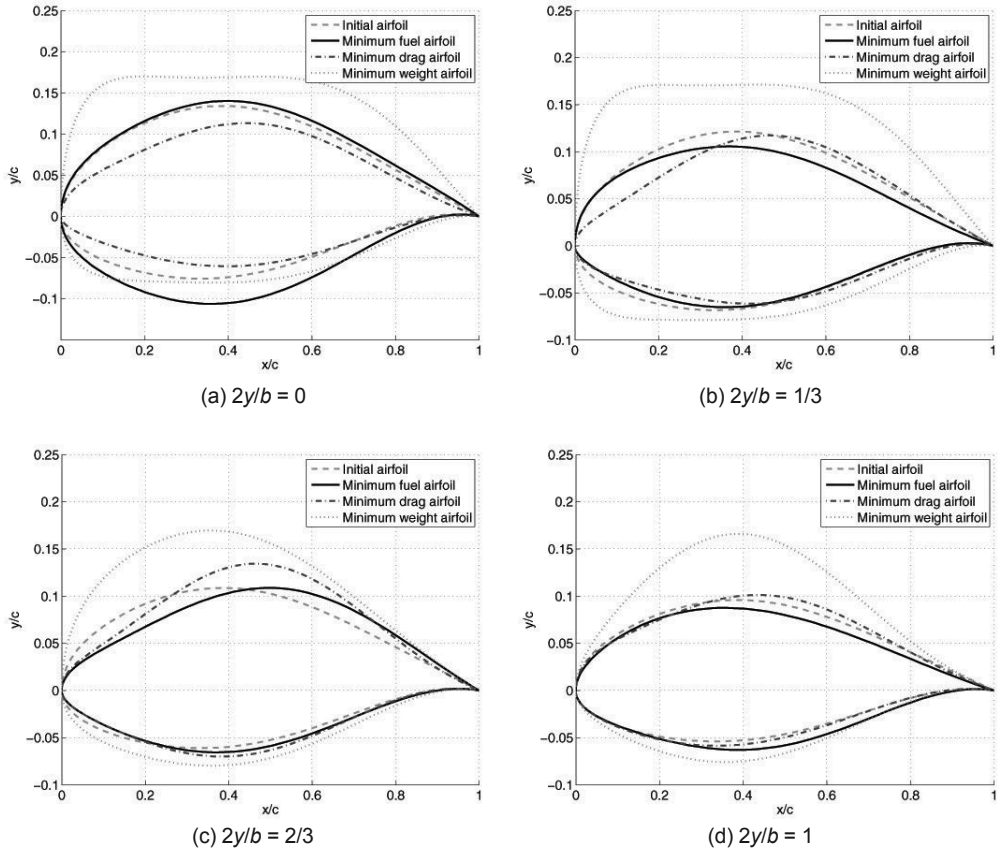


Figure 20. Wing sections of the subsonic wing optimised for minimum fuel weight.

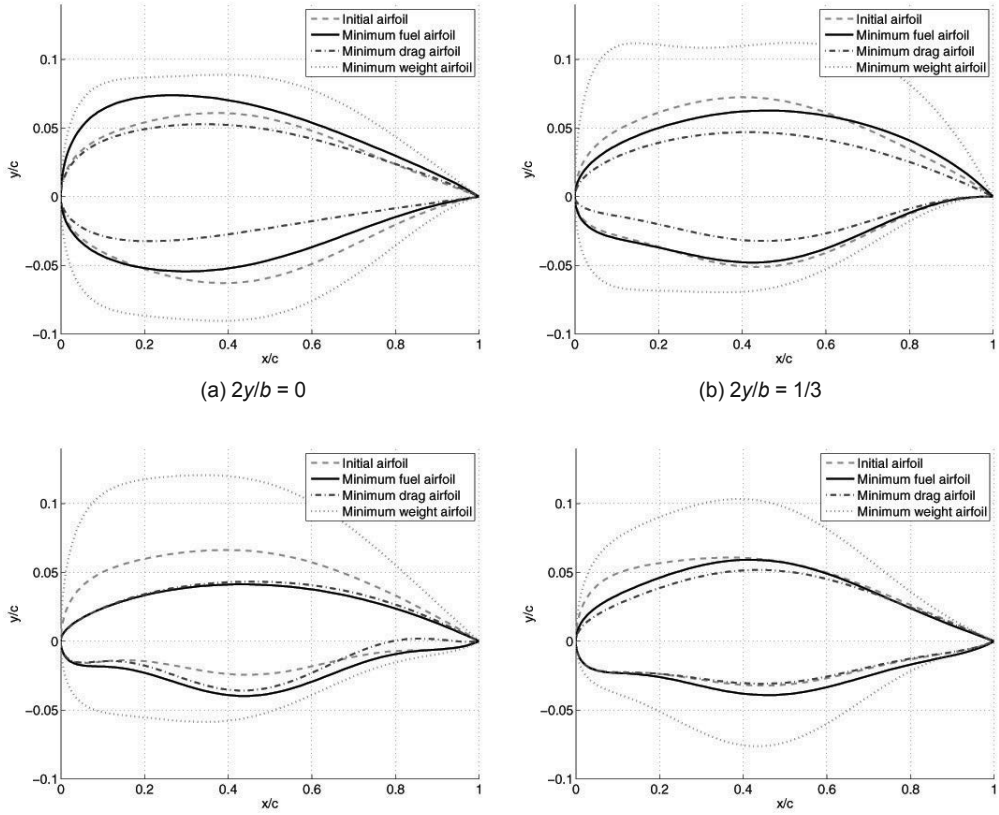
and lower surface of the three subsonic wings (the reference wing, the wing with minimum drag and the wing with minimum fuel weight) are compared to each other in Fig. 22. The contours of pressure coefficient on the upper surface of the wing optimised for minimum fuel weight are shown in Fig. 28(a) and can be compared to the contours of pressure coefficient of the reference wing and the wing optimised for minimum drag shown in Fig. 14.

4.5 Effect of using composite material on the optimum wing shape

In order to investigate the effect of using various materials in the wing-box structure on the optimum wing shape, the same optimisation has been performed but with CFRP composite materials in the wing-box structure. In order to estimate the wing-box weight, the layup of the composite structure must be selected.

Based on the weight estimation technique presented in Section 2, the best layup for the equivalent panels (the layup which results in minimum weight) can be determined. In the structural sizing method, the upper and lower equivalent panels are sized for the maximum allowable normal stress, while the spars webs are sized for maximum allowable shear stress. In order to maximise the allowable normal stress in a composite layup, the ratio of the number of plies in zero degree orientation to the number of total plies should be maximised. On the other hand, the maximum allowable shear stress is achieved in a layup with maximum plies in ±45°. Based on the 10%

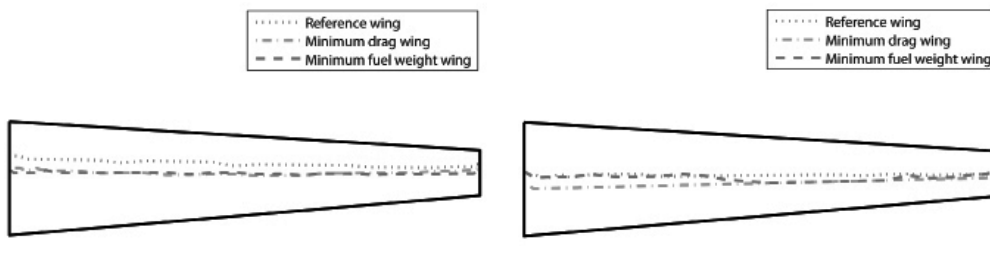
https://doi.org/10.1017/S0001924000008903 Published online by Cambridge University Press



(a) $2y/b = 0$ (b) $2y/b = 1/3$

(c) $2y/b = 2/3$ (d) $2y/b = 1$

Figure 21. Wing sections of the transonic wing optimised for minimum fuel weight.



(a) Wing upper surface (b) Wing lower surface

Figure 22. Boundary layer transition line on three wings.

rule[24], there should be minimum of 12% and maximum of 50% of plies in both 0° and 90° orientations. The percentage of the plies in ±45° should be kept between 24% and 76%. Figure 23 from Ref. 24 shows the area of the preferred fibre pattern. Beside that, based on the design guidelines provided by Ref. 10 the laminate should be symmetric and balanced. Using these guidelines the best layups for the lower surface (under tension) and the spars webs (under shear) can be determined (see Table 6).

https://doi.org/10.1017/S0001924000008903 Published online by Cambridge University Press

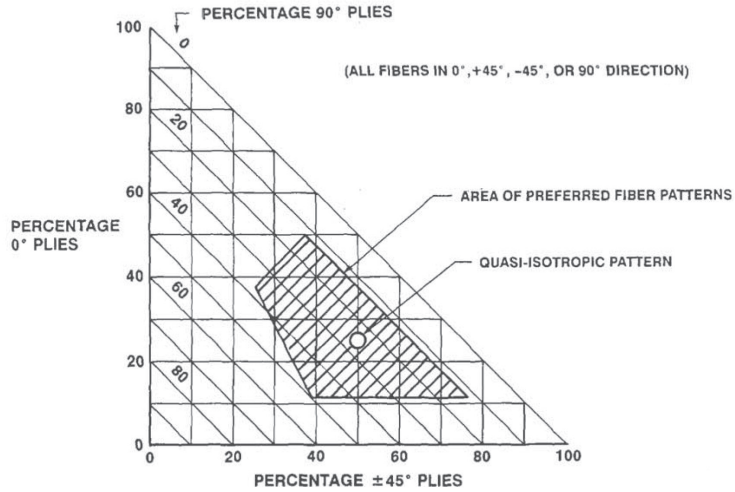


Figure 23. Preferred fibre patterns for fibrous composite laminates[24].

Table 6
Best layups for the panels under tension and the panels under shear.

	Plies % at:		
	0	**±45**	**90**
Panels under tension	50	38	12
Panels under shear	12	76	12

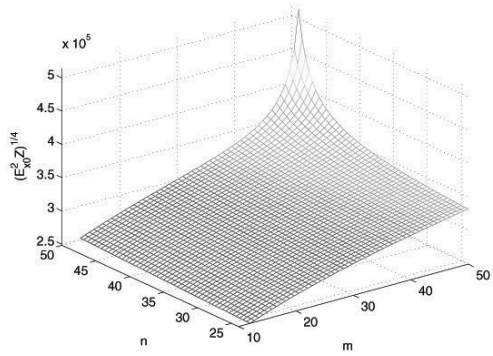


Figure 24. Values of $(E^2_{x0} Z)^{1/4}$ as a function of m and n.

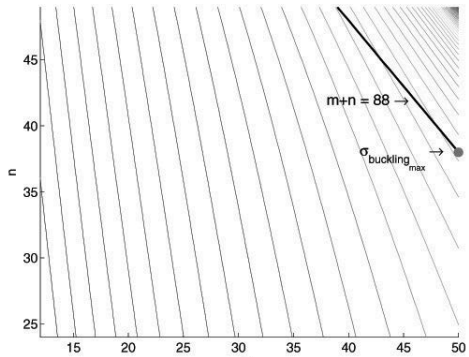


Figure 25. Contours of $(E^2_{x0} Z)^{1/4}$.

In order to find the best layup for the equivalent panels which are under compression, Equation (24) is used. Based on this equation, for a given stiffened panel (F, P and L are known), the buckling stress is maximum when $(E^2_{x0} Z)^{1/4}$ is maximum. Figure 24 shows the value of $(E^2_{x0} Z)^{1/4}$ as a function of the percentage of plies in 0 (m) and ±45(n) directions. The contours of $(E^2_{x0} Z)^{1/4}$ are plotted in Fig. 25. Based on the 10% rule, the sum of m and n should not exceed 88 (minimum 12% of plies must be in 90° orientation). Applying this constraint, the maximum buckling stress is achieved with $m = 50$ and $n = 38$. It is the same layup as the one for maximum allowable tensile stress.

https://doi.org/10.1017/S0001924000008903 Published online by Cambridge University Press

Table 7
Weight comparison for wing-box structure

$$\frac{W_{composite}}{W_{aluminium}}$$

	Quasi-isotropic	Best layup	$m = n = 44$
Subsonic aircraft	1·02	0·61	0·73
Transonic aircraft	1·06	0·63	0·72

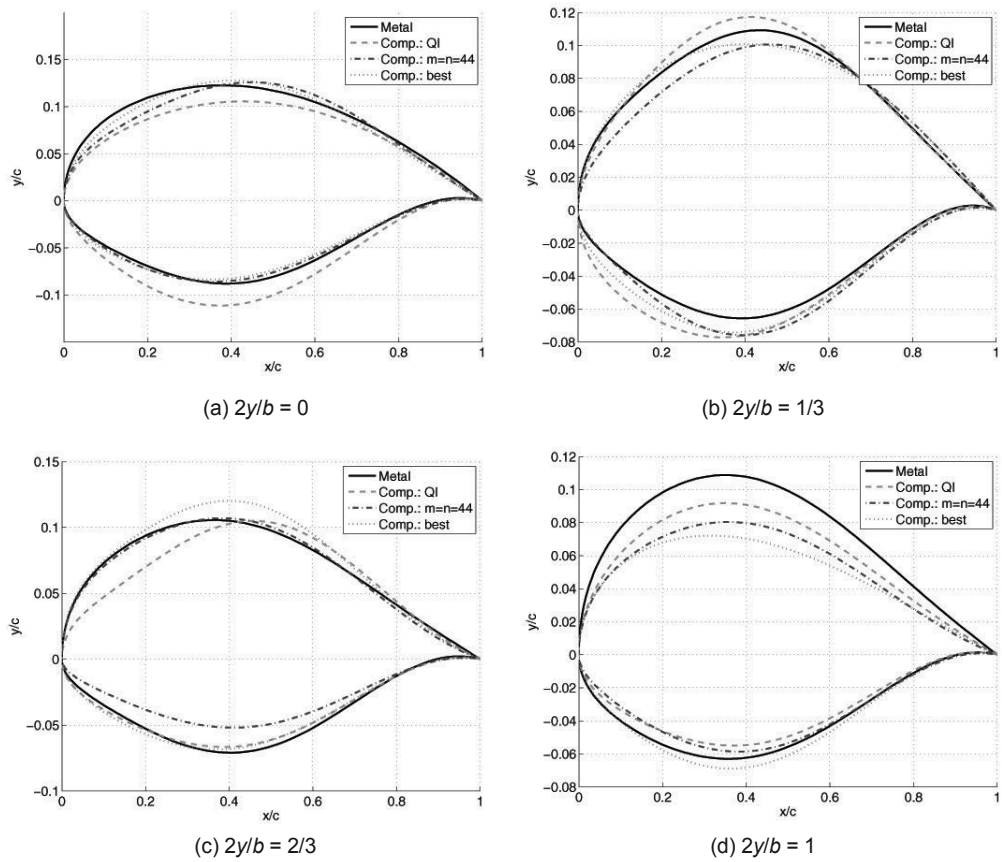
Table 8
Results of wing shape optimisation using various composite layups in wing-box structure

	Subsonic aircraft				Transonic aircraft			
	Reference	QI	$m = n = 44$	best	Reference	QI	$m = n = 44$	best
W_{fuel} (kg)	4,045	3,967	3,869	3,880	7,312	6,648	6,504	6,468
W_{wing} (kg)	2,067	2,066	1,770	1,645	4,677	4,827	4,151	3,965
MTOW (kg)	20,867	20,788	20,393	20,280	43,144	42,630	41,809	41,588

The weight ratio of the composite wing-box and the wing-box made of aluminium alloys is presented in Table 7 for those two mentioned aircraft in the previous section. Three different layups are tested. In the first case, a quasi-isotropic layup is selected for all the equivalent panels (upper equivalent, lower equivalent, front and rear spars webs). The weight of the composite wing-box is calculated to be slightly higher than the weight of the metal wing-box. This result is in line with the experiments[10]. For the quasi-isotropic layup to save weight one should account for changes in the design where fasteners and brackets are eliminated due to co-curing (non-optimum weight). If this is taken into account, the quasi-isotropic layup results in a 10-15% lighter wing-box than the aluminum ones, otherwise it is the same weight or slightly higher[10], which is what we have.

The second case is the best layup. The weight ratio is 0·61 and 0·63 for the subsonic and transonic aircraft respectively. These weights seem lighter than what can be achieved in a real design. Experience has shown that such weight reductions are only achievable for some special cases in terms of loading type or in terms of bad baseline designs in aluminum, for which it is easy to get very light composite alternatives[34,37]. For typical laminates in realistic situations, the ratio is close to 0·7-0·75[33]. The reason is that a significant portion of the structure (typically 10-15%) is designed by out-of-plane strength, in which the composites do not function well. Such structures are dominated by the fittings and 3D connections. In these cases composites would pay a penalty or, at best, would break even. Beside that, the number of unidirectional plies with same orientation next to each other should be limited. In the case of having a number of unidirectional plies in a same direction a matrix crack can easily grow in the matrix and extend from one end of the identical ply stack to the other without being arrested. It is recommended to avoid ply stacks of the same ply orientation that exeed 0·6-0·8 mm (corresponding to 4-5 plies for typical unidirectional materials)[10]. Therefore the best layup seems to be unrealistic. In the third case a more realistic layup with $m = n = 44$ in all four panels is tested. The resulted weight ratio is 0·73 and 0·72 for subsonic and transonic aircraft respectively.

https://doi.org/10.1017/S0001924000008903 Published online by Cambridge University Press



(a) $2y/b = 0$ (b) $2y/b = 1/3$

(c) $2y/b = 2/3$ (d) $2y/b = 1$

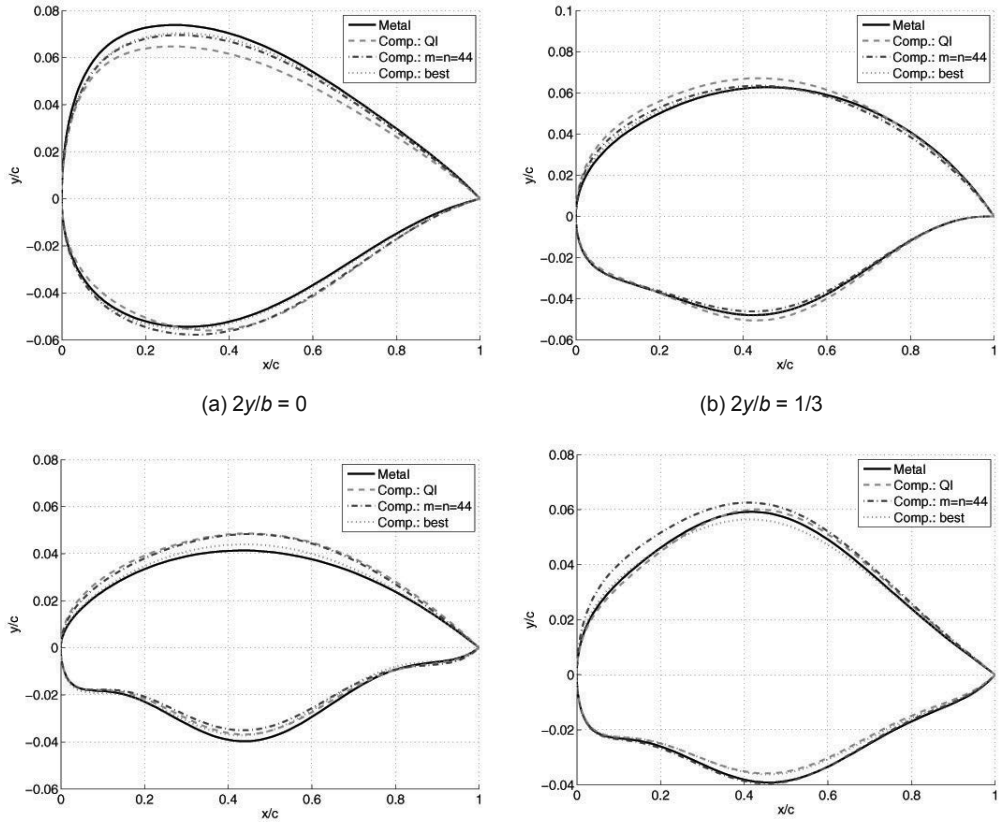
Figure 26. Wing sections of the subsonic wing optimised using various materials in wing-box structure.

The three layups are used for a series of optimisations. The same objective function and constraints as Section 4.4 are used. Table 8 shows the results of these optimisations for both subsonic and transonic aircraft. The optimum wing shape of various layups are compared to each other and to the optimum shape of the metal wing-box in Figs 26 and 27. The contours of pressure coefficient on the upper surface of the optimised wings are shown in Fig. 28.

5.0 CONCLUSION

A quasi analytical method for weight estimation of aircraft wing is presented. This method uses elementary structural analysis of the wing-box structure to estimate the optimum wing-box structural weight. The method is validated and shows a high level of accuracy and a short computational time, which makes it very suitable to be used in multidisciplinary design optimisation tasks. The novelty of the proposed method, is using an accurate method for calculation of the aerofoil effective distance. A mathematical equation is used to relate the wing outer geometry to its structural weight. This method is used for multidisciplinary design optimisation of the wing outer shape. A series of optimisations has been applied to optimise the wing shape using various objective functions. The wing shape optimised for minimum fuel weight is compared to the shapes optimised for minimum aerodynamic drag and minimum structural weight. This comparison shows two guidelines for

https://doi.org/10.1017/S0001924000008903 Published online by Cambridge University Press



(a) 2*y*/*b* = 0

(b) 2*y*/*b* = 1/3

(c) 2*y*/*b* = 2/3

(d) 2*y*/*b* = 1

Figure 27. Wing sections of the transonic wing optimised for minimum fuel weight using various materials in wing-box structure.

wing shape optimisation: (1) a pure aerodynamic optimisation, may not result in the minimum fuel consumption because minimising drag might increase the structural weight; (2) in a wing shape optimisation for minimum fuel consumption, the effect of wing aerofoils shape on the wing structural weight must be taken into account.

The effect of wing-box structural weight on the optimum wing outer shape is investigated. The optimum wing shape of a metal wing is compared to the optimum wing shape of wings made of composites with different layups. The results shows that the optimum aerofoils for a wing constructed using metal alloys are different from the optimum aerofoils for a composite wings. Beside that, the layup of the composites used in the wing-box structure also affect the shape of the optimum aerofoils.

ACKNOWLEDGMENT

The authors like to express their gratitude to National Aerospace Laboratory (NLR) for providing MATRICS-V code. They are also thankful to Dr. Christos Kassapoglou for his support and valuable feedback.

https://doi.org/10.1017/S0001924000008903 Published online by Cambridge University Press

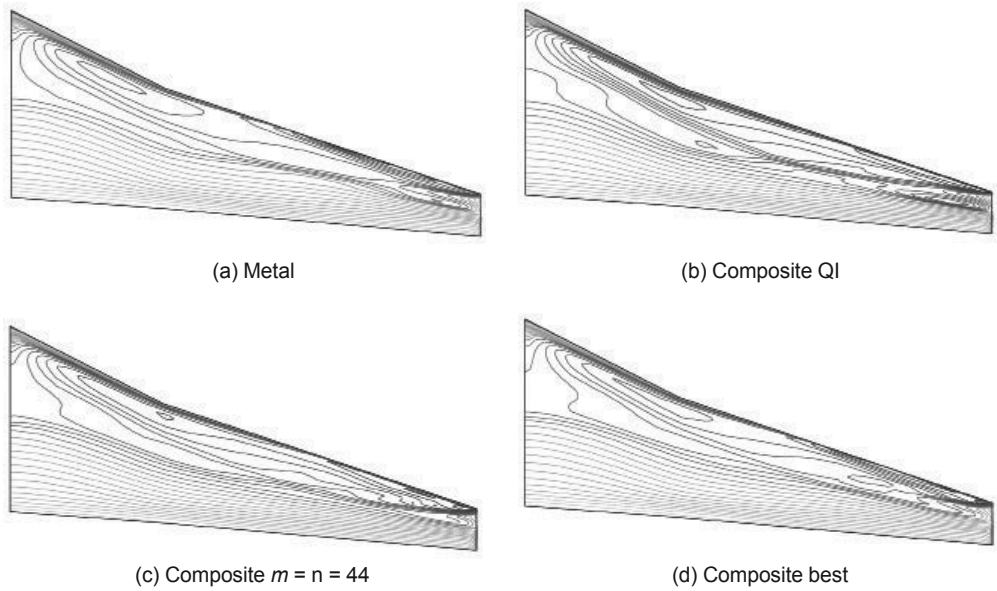


Figure 28. Contour of pressure coefficient on the upper surfaces of the optimised wings for minimum fuel weight.

REFERENCES

1. ANDERSON, J.D. *Fundamentals of Aerodynamics*, Fifth edition, 2011, McGraw-Hill, New York, USA.
2. ARDEMA, M.D., CHAMBERS, M.C., PATRON, A.P., HAHN, A.S., MIURA, H. and MOORE, M.D. Analytical fuselage and wing weight estimation of transport aircraft, 1996, NASA Technical Memorandum 110392.
3. BINDOLINO, G., GHIRINGHELLI, G. RICCI, S. and TERRANEO, M. Multilevel structural optimization for preliminary wing-box weight estimation, *J Aircr*, 2010, **47**, (2), pp 475-489.
4. BUCKLEY, H.P., ZHOU, B.Y. and ZINGG, D.W. Airfoil optimization using practical aerodynamic design requirements, *J Aircr*, 2010, **47**, (5), pp 1707-1719.
5. BURT, M.E. Weight prediction for wings of box construction, 1955, Report 186, RAE.
6. DROEGKAMP, M. Finite element model weight estimation, 1992, SAWE Paper 2089.
7. HOWE, D. *Aircraft Conceptual Design Synthesis*, 2000, Professional Engineering Pub, London, UK.
8. HOWE, D. Aircraft loading and structural layout, 2004, AIAA education series, American Institute of Aeronautics and Astronautics, Reston, VA, USA.
9. HURLIMANN, F., KELM, R., DUGAS, M., OLTMANN, K. and KRESS, G. Mass estimation of transport aircraft wingbox structures with a CAD/CAE-based multidisciplinary process, *Aerospace Sci and Tech*, 2011, **15**, (4), pp 323-333.
10. KASSAPOGLOU, C. Design and analysis of composite structures: with applications to aerospace structures,, First edition, 2010, AIAA education series, American Institute of Aeronautics and Astronautics, Reston, VA, USA.
11. KELM, R., LAPPLE, M. and GRABIETZ, M. Wing primary weight estimation of transport aircrafts in the pre-development phase, 1995, SAWE Paper 2283.
12. LABAN, M., ARENDSEN, P., ROUWHORST, W.F.J.A. and VANKAN, W.J. A Computational design engine for multidisciplinary optimisation with application to a blended wing body configuration, 2002, AIAA paper 91-5058, Ninth AIAA/ISSMO Symposium on Multidisciplinary Analysis and Optimisation, Atlanta, USA
13. LEUNG, T.M. and ZINGG, D.W. Aerodynamic shape optimization of wings using a parallel Newton-Krylov approach, *AIAA J*, 2012, **50**, (3), pp 540-550.

https://doi.org/10.1017/S0001924000008903 Published online by Cambridge University Press

14. MACCI, S.H. Semi-analytical method for predicting wing structural mass, 1995, SAWE Paper 2282.
15. NIU, M.C.Y. *Airframe Stress Analysis and Sizing*, 1997, Conmilit Press, Hong Kong.
16. RAYMER, D.P. Aircraft design : a conceptual approach of AIAA education series, Fifth edition, 2012, American Institute of Aeronautics and Astronautics, Reston, VA, USA.
17. SENSMEIER, M.D., STEWART, B.T. and SAMAREH, J.A. Rapid generation and assessment of aircraft structural topologies for multidisciplinary optimization and weight estimation, 2006, AAAI Paper 2006-1981.
18. SHANLEY, F.R. Weight-strength analysis of aircraft structures, 1950, Dover Publication, New York, USA.
19. TOAL, D.J.J. and KEANE, A.J. Efficient multipoint aerodynamic design optimization via cokriging, *J Aircr*, 2011, **48**, (5), pp 1685-1695.
20. TORENBEEK, E. Development and application of a comprehensive, design-sensitive weight prediction method for wing structures of transport category aircraft, Report, LR-693, Delft University of Technology, Delft (Netherlands), 1992.
21. TORENBEEK, E. *Synthesis of Subsonic Airplane Design*, 1982, Delft University Press.
22. ZHANG, Z. and LUM, K.Y. Airfoil optimization design of drag minimization with lift constraint using adjoint equation method, 2006, AAAI Paper 2006-55.
23. MIL-HDBK-5H, *Military Handbook, Metalic Materials and Elements for Aerospace Vehicle Structures*, December 1998.
24. Douglas Aircraft Company, McDonnell Douglas Corporation, The ten-percent rule for preliminary sizing of fibrous composite structures, 1992, SAWE Paper 2054.
25. DRELA, M. and YOUNGREN, H. AVL (Athena Vortex Lattice) 3.26, 2006, Massachusetts Institute of Technology.
26. ELHAM, A., LA ROCCA, G. and VOS, R. Refined preliminary weight estimation tool for airplane wing and tail, 2011, SAE Technical paper 2011-01-2765.
27. KULFAN, B.M. Universal parametric geometry representation method, *J Aircr*, 2008, **45**, (1), pp 142-158.
28. MEGSON, T.H.G. Aircraft structures for engineering students, Elsevier aerospace engineering series, Fourth edition, 2007, Butterworth-Heinemann, Oxford, Burlington, MA, USA
29. NIU, M.C.Y. *Composite Airframe Structures: Practical Design Information And Data*, 1992, Conmilit Press, Hong Kong.
30. OBERT, E. Aerodynamic design of transport aircraft, 2009, Ios Press, Amsterdam, The Netherlands.
31. ROSKAM, J. Airplane design part I, 1986, DARcorporation, Lawrence, KS, USA.
32. ROSKAM, J. Airplane design part V, DARcorporation, Lawrence, KS, USA.
33 SOUTIS, C. Fibre reinforced composites in aircraft construction, *Prog in Aerospace Sci*, 2005, **41**, (2), pp 143-151.
34. TENNEY, D.R., DAVIS, J.G., PIPES, R.B. and JOHNSTON, N. NASA composite materials development: lessons learned and future challenges, 2009, NATO RTO AVT-164 Workshop on Support of Composite Systems.
35. TERPSTRA, A. Wing Weight Prediction in the Preliminary Design Phase, 2002, MSc thesis, Delft University of Technology.
36. TETLOW, R. Design charts for carbon fiber composites, 1970, Cranfield Memo 9.
37. VASILIEV, V.V. and RAZIN, A.F. Anisogrid composite lattice structures for spacecraft and aircraft applications, *Composite Structures*, 2006, **76**, (1-2), pp 182-189.
38. VAN DER WEES, A.J., VAN MUIJDEN, J. and VAN DER VOOREN, J. A Fast and robust viscous-inviscid interaction solver for transonic flow about wing/body configurations on the basis of full potential theory, 1996, AIAA-93-3026, AIAA 24th Fluid Dynamics Conference.
39. Matlab optimization toolbox — R2011a, 2011, Mathworks.
40. ELHAM, A. and VAN TOOREN, M. Weight indexing for airfoil multi-objective optimization, *J Aircr,* July/Aug 2013, **50**, (4) pp 1046-1049.

https://doi.org/10.1017/S0001924000008903 Published online by Cambridge University Press